

Equilibration processes in the Warm-Hot Intergalactic Medium

A.M. Bykov · F.B.S. Paerels · V. Petrosian

Received: 17 September 2007; Accepted: 30 October 2007

Abstract The Warm-Hot Intergalactic Medium (WHIM) is thought to contribute about 40 – 50 % to the baryonic budget at the present evolution stage of the universe. The observed large scale structure is likely to be due to gravitational growth of density fluctuations in the post-inflation era. The evolving cosmic web is governed by non-linear gravitational growth of the initially weak density fluctuations in the dark energy dominated cosmology. Non-linear structure formation, accretion and merging processes, star forming and AGN activity produce gas shocks in the WHIM. Shock waves are converting a fraction of the gravitation power to thermal and non-thermal emission of baryonic/leptonic matter. They provide the most likely way to power the luminous matter in the WHIM. The plasma shocks in the WHIM are expected to be collisionless. Collisionless shocks produce a highly non-equilibrium state with anisotropic temperatures and a large differences in ion and electron temperatures. We discuss the ion and electron heating by the collisionless shocks and then review the plasma processes responsible for the Coulomb equilibration and collisional ionisation equilibrium of oxygen ions in the WHIM. MHD-turbulence produced by the strong collisionless shocks could provide a sizeable non-thermal contribution to the observed Doppler parameter of the UV line spectra of the WHIM.

Keywords intergalactic medium · shock waves · galaxies: clusters: general

A.M. Bykov
A.F. Ioffe Institute of Physics and Technology, St. Petersburg, 194021, Russia
E-mail: byk@astro.ioffe.ru

F.B.S. Paerels
Columbia Astrophysics Laboratory, Department of Astronomy, Columbia University, 550 West 120th Street, New York, NY 10027
E-mail: frits@astro.columbia.edu

V. Petrosian
Department of Physics, Stanford University, Stanford, CA 94305
E-mail: vahe@astronomy.stanford.edu

1 Introduction

Cosmological simulations of the large-scale structure (LSS) predict that about 40–50 % of baryons at epoch $z < 2$ could reside in the Warm-Hot Intergalactic Medium (WHIM) with temperatures 10^5 – 10^7 K at moderate overdensities $\delta < 100$ (Cen & Ostriker 1999; Davé et al. 2001; Fang et al. 2002). The WHIM heating is due to shocks driven by gravitationally accelerated flows in the LSS structure formation scenario (e.g. Kang et al. 2007). Numerical simulations predict the observational signatures of the web gas as a function of redshift. The simulations account for feedback interactions between galaxies and the intergalactic medium, and demonstrate that the X-ray and ultraviolet O VI, O VII and O VIII lines and the H I Lyman alpha line are good tracers of low-density cosmic web filamentary structures (e.g. Hellsten et al. 1998; Tripp et al. 2000; Cen et al. 2001; Furlanetto et al. 2004). Intervening metal absorption systems of highly ionised C, N, O, Ne in the soft X-ray spectra of bright Active Galactic Nuclei (AGN) were suggested to be tracer of the WHIM. The predicted distribution of ion column densities in the WHIM absorbers is steep enough to provide only a few systems with $N_{\text{O VII}} > 10^{15} \text{ cm}^{-2}$ along an arbitrary chosen line of sight (e.g. Fang et al. 2002). Therefore, the detection of the WHIM is particularly difficult and requires very sensitive UV and X-ray detectors, both for absorption and for emission processes (e.g. Lehner et al. 2007; Nicastro et al. 2005; Kaastra et al. 2006; Takei et al. 2007 and Richter et al. 2008; Durret et al. 2008 - Chapters 3 and 4, this volume). Future projects and namely *Cosmic Origin Spectrograph* (COS), the *X-Ray Evolving Universe Spectrometer* (XEUS), *Constellation-X* and the *Diffuse Intergalactic Oxygen Surveyor* (DIOS) will increase the signal-to-noise ratio in the spectra allowing to study weak systems with $N_{\text{H I}} < 10^{12.5} \text{ cm}^{-2}$ and $N_{\text{O VII}} < 10^{15} \text{ cm}^{-2}$. Simulations of spectra of the broad Ly α absorption lines and the highly ionised oxygen lines in the weak systems require thorough modelling of physical condition in the plasma (see e.g. Mewe 1990; Paerels & Kahn 2003; Kawahara et al. 2006). We discuss in this paper the heating and equilibration processes in the shocked WHIM plasma affecting the spectral simulations. A discussion of collisionless shock physics relevant to cosmological shocks in the WHIM can be found in Bykov et al. 2008 - Chapter 7, this volume. To this end, in this paper we discuss first some specific features of collisionless shock heating of ions of different charge states providing highly non-equilibrium initial states just behind the magnetic ramp region that relaxes to an equilibrium state through Coulomb collisions, and the relation of the processes to simulations of emission/absorption spectra of the WHIM and observational data analysis.

2 WHIM heating and ion temperature evolution

The plasma ion heating in the WHIM is most likely due to cosmological shocks. The Alfvén Mach number of a shock propagating through an ionised gas of local overdensity $\delta = \rho / \langle \rho \rangle$ at the epoch z in the standard Λ CDM cosmology is determined by

$$\mathcal{M}_a = v_{\text{sh}}(4\pi\rho_i)^{1/2}/B \approx 20.6 v_{s7}\delta^{1/2}(1+z)^{3/2}(\Omega_b h^2/0.02)^{1/2}B_{-9}^{-1}, \quad (1)$$

where B_{-9} is the magnetic field just before the shock, measured in nG and v_{s7} is the shock velocity in 10^7 cm s^{-1} , and $\langle \rho \rangle$ is the average density in the Universe.

The sonic Mach number for a shock propagating in a plasma of standard cosmic abundance is

$$\mathcal{M}_s \approx 8.5 v_{s7} [T_4(1 + f_{ei})]^{-1/2}, \quad (2)$$

where T_4 is the plasma ion temperature measured in 10^4 K (typical for a preshock photoionised plasma) and $f_{ei} = T_e/T_i$. An important plasma parameter is

$$\beta = \mathcal{M}_a^2/\mathcal{M}_s^2 \approx 6\delta(1+z)^3(\Omega_b h^2/0.02)B_{-9}^{-2}[T_4(1+f_{ei})].$$

It is the ratio of the thermal and magnetic pressures. In hot X-ray clusters of galaxies the beta parameter is ~ 100 for $\sim \mu\text{G}$ magnetic fields in the clusters. The most uncertain parameter is the magnetic field value in the WHIM allowing for both $\beta \sim 1$ and $\beta \gg 1$ cases.

In a supercritical collisionless shock the conversion of kinetic energy of an initially cold flow to the ion distribution with high kinetic temperature occurs in the thin ion viscous jump. The width of the ion viscous jump Δ_{vi} in a collisionless shock propagating through a plasma with $\beta \sim 1$ is typically of the order of a ten to a hundred times of the ion inertial length l_i defined as $l_i = c/\omega_{pi} \approx 2.3 \times 10^7 n^{-0.5}$ cm. Here ω_{pi} is the ion plasma frequency. The ion inertial length in the WHIM can be estimated as

$$l_i \approx 5.1 \times 10^{10} \delta^{-1/2} (1+z)^{-3/2} (\Omega_b h^2/0.02)^{-1/2} \text{ cm.}$$

The width of the shock transition region for magnetic field is also $\gtrsim 10l_i$ for a quasi-perpendicular shock, but it is often about ten times wider for quasi-parallel shocks.

Properties of nonrelativistic shocks in a hot, low magnetised plasma with high $\beta \gg 1$ are yet poorly studied. Measurements from the *ISEE 1* and *ISEE 2* spacecrafts were used by Farris et al. (1992) to examine the terrestrial bow shock under high beta conditions. These measurements were compared with and found to be in agreement with the predicted values of the Rankine-Hugoniot relations using the simple adiabatic approximation and a ratio of specific heats, γ , of 5/3. Large magnetic field and density fluctuations were observed, but average downstream plasma conditions well away from the shock were relatively steady, near the predicted Rankine-Hugoniot values. The magnetic disturbances persisted well downstream and a hot, dense ion beam was detected leaking from the downstream region of the shock. The observation proved the existence of collisionless shocks in high beta plasma, but a detailed study of high beta shock structure is needed for cosmological plasmas.

We discuss in the next section the ion heating in collisionless shocks illustrating the most important features of the process with the results of a hybrid simulation of the oxygen ions heating in a quasi-perpendicular shock considered earlier by Bykov et al. 2008 - Chapter 7, this volume.

2.1 Collisionless shock heating of the ions

Ion heating mechanisms in collisionless shocks depend on the shock Alfvén Mach number, the magnetic field inclination angle (θ_n), plasma parameter β and the composition of the incoming plasma flow. The structure of a supercritical shock is governed by the ion flows instabilities (see e.g. Kennel et al. 1985; Lembedge et al. 2004; Burgess et al. 2005). In a quasi-parallel shock ($\theta_n \lesssim 45^\circ$) a mixed effect of a sizeable backstreaming ion fraction and the ions scattered by the strong magnetic field fluctuations (filling the wide shock transition region) results in the heating of ions in the downstream region.

The ions reflected and slowed down by an electric potential jump $\delta\phi$ at the shock ramp of a quasi-perpendicular ($\theta_n \gtrsim 45^\circ$) shock constitute a multi-stream distribution just behind a relatively thin magnetic ramp as it is seen in Fig. 1 and Fig. 2 (left panel). The O VII phase densities and distribution functions were simulated with a hybrid code for a quasi-perpendicular ($\theta_n = 80^\circ$) shock in a hydrogen-helium dominated plasma (see Bykov et al. 2008 - Chapter 7, this volume). Phase densities $x-v_x$, $x-v_y$, $x-v_z$ of the O VII ion are shown in Fig. 1 in the reference frame where the particle reflecting wall (at far right) is at rest and the shock is moving. The shock is propagating along the x -axis from the left to the right and the magnetic field is in the x - z plane. The system is periodic in the y dimension. The incoming plasma beam in the simulation was composed of protons (90 %), alpha particles (9.9 %) and a dynamically insignificant fraction of oxygen ions (O VII) with the upstream plasma parameter $\beta \sim 1$. The ions do not change their initial charge states in a few gyro-periods while crossing the cosmological shock ramp where the Coulomb interactions are negligible.

The simulated data in Fig. 1 show the ion velocities phase mixing resulting in a thermal-like broad ion distribution at a distance of some hundreds of ion inertial lengths in the shock downstream (see the right panel in Fig. 2). It is also clear in Fig. 1 that the shocked ion distribution tends to have anisotropy of the effective temperature. The temperature anisotropy $T_\perp \sim 3 T_\parallel$ relative to the magnetic field was found in that simulation. Moreover, the hybrid simulation shows that the T_\perp of the O VII is about 25 times higher than the effective perpendicular temperature of the protons. Thus the ion downstream temperature declines from the linear dependence on the ion mass. The simulations show excessive heating of heavy ions in comparison with protons.

Lee & Wu (2000) proposed a simplified analytical model to estimate the ion perpendicular temperature dependence on Z/A , where $m_i = Am_p$. Specifically, the model predicts the ratio of the ion gyration velocity v_{ig2} in the downstream of a perpendicular shock ($\theta_n \sim 90^\circ$) to the velocity of the incident ion in the shock upstream, v_1 ,

$$\frac{v_{ig2}}{v_1} = \left| \left(1 - \alpha \frac{Z}{A} \right)^{1/2} - \frac{B_{t1}}{B_{t2}} \right|, \quad (3)$$

where $\alpha = 2e\delta\phi/m_p v_1^2 < 1$, and the potential jump $\delta\phi$ is calculated in the shock normal frame (see Lee & Wu 2000). The model is valid for the ions with gyroradii larger than the shock transition width Δ_{vi} . It is not a fair approximation for the protons, but it is much better for temperature estimation of heavy ions just behind the shock magnetic ramp. The model of ion heating in the fast, supercritical quasi-perpendicular ($\theta_n \gtrsim 45^\circ$) shocks of $\mathcal{M}_a \gtrsim 3$ predicts a higher downstream perpendicular temperature for the ions with larger A/Z .

2.2 Collisionless heating of the electrons

The initial electron temperature just behind the viscous ion jump of a cosmological shock depends on the collisionless heating of the electrons. The only direct measurements of the electron heating by collisionless shocks are those in the Heliosphere. The interplanetary shock data compiled by Schwartz et al. (1988) show a modest, though systematic departure of the electron heating from that which would result from the approximately constant ratio of the perpendicular temperature to the magnetic field

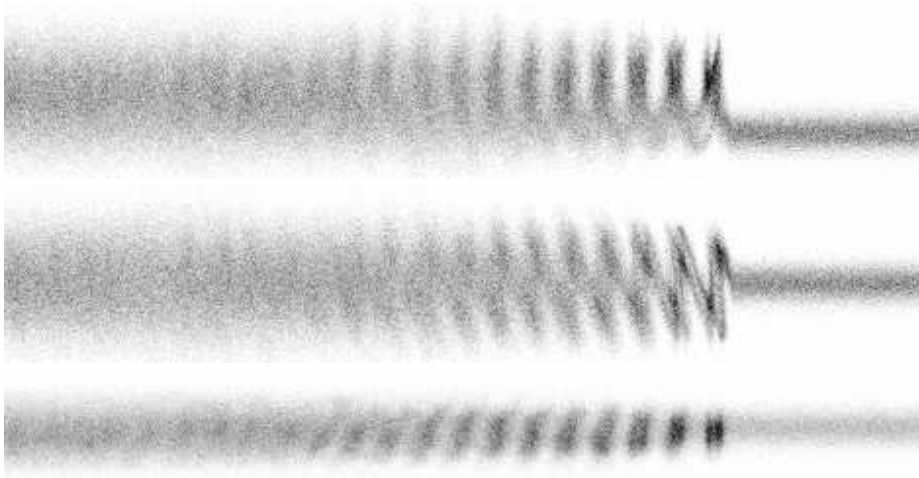


Fig. 1 O VII phase density in a hybrid simulated quasi-perpendicular shock (80° inclination). The shock is moving from left to right in the reference frame where the particle reflecting wall is at rest. The figures show the oxygen phase densities in $x - v_x$, $x - v_y$ and $x - v_z$ projections from top to bottom respectively. The size of the simulation box in x-dimension is about $300 l_i$.

strength (i.e. adiabatic heating). Thus, some modest non-adiabatic electron collisionless heating is likely present. In the case of a nonradiative supernova shock propagating through *partially ionised* interstellar medium the ratio T_e/T_i in a thin layer (typically $< 10^{17}$ cm) just behind a shock can be tested using the optical diagnostics of broad and narrow Balmer lines (e.g. Raymond 2001). High resolution *Hubble Space Telescope* (*HST*) Supernova remant (SNR) images make that approach rather attractive. A simple scaling $T_e/T_i \propto v_{\text{sh}}^{-2}$ was suggested by Ghavamian et al. (2007) to be consistent with the optical observations of SNRs.

Strong shocks are thought to transfer a sizeable fraction of the bulk kinetic energy of the flow into large amplitude nonlinear waves in the magnetic ramp region. The thermal electron velocities in the ambient medium are higher than the shock speed if the shock Mach number $\mathcal{M}_s < \sqrt{m_p/m_e}$, allowing for a nearly-isotropic angular distribution of the electrons. Non-resonant interactions of these electrons with large-amplitude turbulent fluctuations in the shock transition region could result in collisionless heating and pre-acceleration of the electrons (Bykov & Uvarov 1999; Bykov 2005). They calculated the electron energy spectrum in the vicinity of the shock waves and showed that the heating and pre-acceleration of the electrons occur on a scale of the order of several hundred ion inertial lengths in the vicinity of the viscous discontinuity. Although the electron distribution function is in a significantly non-equilibrium state near the shock front, its low energy part can be approximated by a Maxwellian distribution. The effective electron temperature just behind the front, obtained in this manner, increases with the shock wave velocity as $T_e \propto v_{\text{sh}}^b$ with $b \leq 2$. They also showed that if the electron transport in the shock transition region is due to turbulent advection by strong vortex fluctuations of the scale of about the ion inertial length, then the nonresonant electron heating is rather slow (i.e. $b \leq 0.5$). The highly developed vortex-type

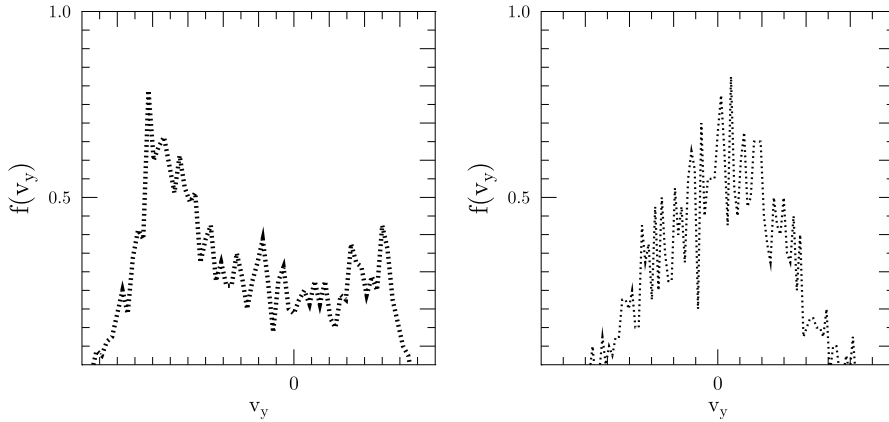


Fig. 2 Hybrid simulated O VII distribution function (normalised) as a function of a random velocity component $\delta v_y = v_y - \langle v_y \rangle$ transverse to the downstream magnetic field in a quasi-perpendicular shock (80° inclination). The shock propagates along the x -axis, while the initial regular magnetic field is in the x - z plane. In the left panel the distribution in the viscous velocity jump is shown. The right panel shows the distribution behind the jump at the position of the left end in Fig. 1. Multi-velocity structure of the flow is clearly seen in the left panel, while it is relaxing to quasi-Maxwellian in the right panel.

turbulence is expected to be present in the transition regions of very strong shocks. That would imply that the initial $T_e/T_i \propto v_{\text{sh}}^{(b-a)}$ just behind the transition region would decrease with the shock velocity for $\mathcal{M}_s \gg 1$. Here the index a is defined by the relation $T_i \propto v_{\text{sh}}^a$ for a strong shock. The degree of electron-ion equilibration in a collisionless shock is a declining function of shock speed. In the case of strong vortex-type turbulence in the shock transition region one expects in the standard ion heating case with $a = 2$ and rather small b to have $(a - b) \lesssim 2$. That T_e/T_i scaling is somewhat flatter, but roughly consistent with, that advocated by Ghavamian et al. (2007). On the other hand in a collisionless shock of a moderate strength $\mathcal{M}_s < 10$ the electron transport through the magnetic ramp region could be diffusive, rather than by the turbulent advection by a strong vortices. That results in a larger degree of the collisionless electron heating/equilibration in the shocks as it is shown in Fig. 4 of the paper by Bykov & Uvarov (1999). Recently, Markevitch & Vikhlinin (2007) argued for the collisionless heating/equilibration of the electron temperature in the bow shock of $\mathcal{M}_s \sim 3$ in the 1E 0657 – 56 cluster.

If the local Mach number \mathcal{M}_s of the incoming flow in a strong shock wave exceeds $\sqrt{m_p/m_e}$, which could occur in the cluster accretion shocks, the thermal electron distribution becomes highly anisotropic and high frequency whistler type mode generation effects could become important. Levinson (1996) performed a detailed study of resonant electron acceleration by the whistler mode for fast MHD shock waves. Electron heating and Coulomb relaxation in the strong accretion shocks in clusters of galaxies was discussed in details by Fox & Loeb (1997).

We summarise this section concluding that a collisionless shock produces in the downstream flow a highly non-equilibrium plasma state with strongly different temperatures of the electrons and ions of different species. Moreover, the postshock ion temperatures are anisotropic. The width of the collisionless shock transition region is smaller by many orders of magnitude than the Coulomb mean free path (that is of a kiloparsec range). We consider now the structure and the processes in the postshock Coulomb equilibration layers in the WHIM.

3 Coulomb relaxation of temperatures in the WHIM

3.1 Relaxation of the ion temperature anisotropy

A plasma flow partly randomised just behind the viscous ion jump in a collisionless shock transition has an anisotropic velocity distribution with respect to the mean magnetic field. In Fig. 1 the oxygen phase densities in the $v_x - x$ and $v_y - x$ projections transverse to the mean field have a substantially wider distribution than that in the projection $v_z - x$ parallel to the magnetic field. In many cases the ion velocity distributions (like that in Fig. 2 right) can be approximated with a quasi-Maxwellian distribution introducing some effective kinetic temperature (more exactly it is the second moment of the distribution). Then the parallel and perpendicular (to the mean field) temperatures are different and we approximate the 3D particle distribution as

$$f(v_{\perp}, v_{\parallel}) = \left(\frac{m}{2\pi T_{\perp}}\right) \left(\frac{m}{2\pi T_{\parallel}}\right)^{1/2} \exp\left(-\frac{mv_{\perp}^2}{2T_{\perp}} - \frac{mv_{\parallel}^2}{2T_{\parallel}}\right). \quad (4)$$

We will measure the temperatures in energy units in most of the equations below (thus $k_{\text{B}}T \rightarrow T$). Ichimaru & Rosenbluth (1970) (see also a comment by Kaiser 1979) obtained the following equation to describe the ion anisotropy relaxation

$$\frac{dT_{\perp}}{dt} = -\frac{1}{2} \frac{dT_{\parallel}}{dt} = -\frac{T_{\perp} - T_{\parallel}}{\tau_i}. \quad (5)$$

Here

$$\tau_i^{-1} = \frac{8\pi^{1/2} n_i Z^2 e^4 \ln A}{15 m_i^{1/2} T_{\text{eff}}^{3/2}}, \quad (6)$$

where $\ln A$ is the Coulomb logarithm and the effective ion temperature is defined as

$$\frac{1}{T_{\text{eff}}^{3/2}} = \frac{15}{4} \int_{-1}^1 d\mu \frac{\mu^2 (1 - \mu^2)}{[(1 - \mu^2)T_{\perp} + \mu^2 T_{\parallel}]^{3/2}}. \quad (7)$$

These equations were obtained under the assumption that the electrons have no dynamical role, but provide a static dielectric background to the ions. We can directly apply Eqs. 5–7 to isotropisation of the plasma field particles (i.e. protons in our case). Isotropisation of the minor ion components is mainly due to their interactions with protons and helium because of a low metal number density in cosmic plasma.

3.2 Relaxation of the ion and electron temperatures

Following shock heating and the temperature isotropisation a quasi-Maxwellian distribution will be established within all plasma components, i.e. groups of identical particles, after a time scale given by Eq. 6. The effective temperatures differs strongly between the components. All the plasma particles will undergo Coulomb collisions with the protons, alpha particles and electrons dominating the WHIM plasma, resulting in the temperature equilibration. Spitzer (1962) found that the temperature relaxation of a test particle of type a with plasma field particles can be approximately estimated from

$$\frac{dT_a}{dt} = \frac{T_p - T_a}{\tau_{ap}} \quad (8)$$

where

$$\tau_{ap}^{-1} = \frac{8(2\pi)^{1/2}}{3} \frac{n_p Z^2 e^4 \ln \Lambda}{m_a m_p} \left(\frac{T_p}{m_p} + \frac{T_a}{m_a} \right)^{-3/2} \quad (9)$$

In the thermal equilibrium state the postshock plasma must have a single equilibrium temperature T_{eq} . In a fully ionised plasma without energy exchange with external components (i.e. radiation or plasma wave dissipation) T_{eq} can be found from the condition of constant pressure in the plane shock downstream resulting in

$$T_{eq} = \sum n_a T_{a0} / \sum n_a \quad (10)$$

In cosmic plasmas it is often a fair approximation to estimate T_{eq} from the equation $2T_{eq} = T_e + T_p$. Then following Sivukhin (1966) the charged particle equilibration can be approximately described through the equation

$$\ln \left| \frac{\sqrt{T_e} - \sqrt{T_{eq}}}{\sqrt{T_e} + \sqrt{T_{eq}}} \right| = -\frac{t}{\tau_{eq}} - \frac{2}{3} \left(\frac{T_e}{T_{eq}} \right)^{3/2} - 2 \left(\frac{T_e}{T_{eq}} \right)^{1/2} + C_e, \quad (11)$$

where C_e is a constant to be determined from the initial temperature T_{a0} of a relaxing component $a = e, p$,

$$\tau_{eq}^{-1} \approx \frac{16(2\pi)^{1/2}}{3} \frac{n_p e^4 \ln \Lambda}{m_e m_p} \left(\frac{T_{eq}}{m_e} \right)^{-3/2}. \quad (12)$$

Eq. 11 and Eq. 12 allow to calculate the structure of relaxation layers to be seen behind a collisionless shock in the WHIM. In Fig. 3 we illustrate the postshock equilibration of initially cold electrons with the protons initially heated at the ion viscous jump of a collisionless shock transition. The width of the ion viscous jump in cosmological shocks is negligible compared with the equilibration length $x_{eq} = u_2 \tau_{eq}$, where u_2 is the downstream flow velocity in the shock rest frame. The characteristic column density $N_{eq} = n_2 x_{eq}$ to be traversed by protons and electrons in the downstream plasma (of a number density n_2) before the temperature equilibration, as it follows from Eq. 12, does not depend on the plasma number density, and $N_{eq} \propto v_{sh}^4$. The corresponding shocked WHIM column density can be expressed through the shock velocity v_7 measured in 100 km s^{-1} , assuming a strong shock where $u_2 = v_{sh}/4$:

$$N_{eq} \approx 5 \times 10^{17} v_7^4 [\ln \Lambda]^{-1} \text{ cm}^{-2},$$

or through the shocked WHIM gas temperature T_6 (measured in 10^6 K):

$$N_{eq} \approx 2.5 \times 10^{17} T_6^2 [\ln \Lambda]^{-1} \text{ cm}^{-2}.$$

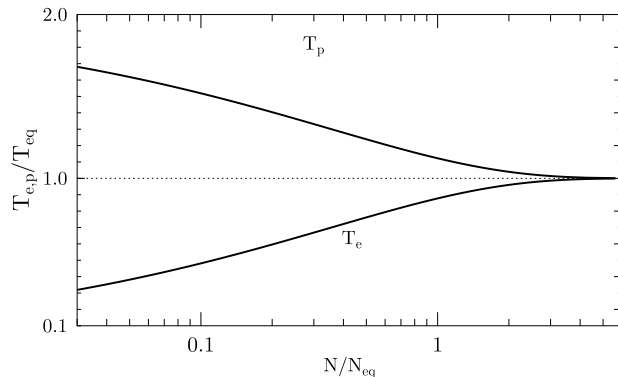


Fig. 3 Postshock temperature equilibration between the ion and electron components due to the Coulomb interactions.

The Coulomb logarithm for the WHIM condition is $\ln A \sim 40$. It follows from Fig. 3 that in the Coulomb relaxation model the postshock plasma column density $N_{\text{H}} > 3N_{\text{eq}}$ ensures the equilibration at a level better than 1 %.

The metal ions can be initially heated at the shock magnetic ramp to high enough temperatures $> AT_{\text{p}}$ (see e.g. Korreck et al. 2007) for a recent analysis of interplanetary collisionless shock observations with *Advanced Composition Explorer*). However, in a typical case the depth $N > 3N_{\text{eq}}$ is enough for the ion temperature equilibration.

To study UV and X-ray spectra of the weak systems ($N_{\text{HI}} < 10^{12.5} \text{ cm}^{-2}$ and $N_{\text{OVII}} < 10^{15} \text{ cm}^{-2}$) modelling of shocked filaments of $N_{\text{H}} \lesssim 10^{17} \text{ cm}^{-2}$ would require an account of non-equilibrium effects of low electron temperature $T_{\text{e}}/T_{\text{eq}} < 1$.

3.3 Effect of postshock plasma micro-turbulence on the line widths

We consider above only the WHIM temperature evolution due to the Coulomb equilibration processes. Shocks producing the WHIM could propagate through inhomogeneous (e.g. clumpy) matter. The interaction of a shock with the density inhomogeneities results in the generation of MHD-waves (Alfvén and magnetosonic) in the shock downstream (see e.g. Vainshtein et al. 1993). The MHD-wave dissipation in the shock downstream could selectively heat ions, being a cause of a non-equilibrium $T_{\text{e}}/T_{\text{i}}$ ratio. In case of a strong collisionless shock propagating in a turbulent medium, cosmic ray acceleration could generate a spectrum of strong MHD-fluctuations (see e.g. Blandford & Eichler 1987; Bell 2004; Vladimirov et al. 2006). These MHD-fluctuations could carry a substantial fraction of the shock ram pressure to the upstream and then to the downstream providing a heating source throughout the downstream. The velocity fluctuations could also produce non-thermal broadening of the lines. The amplitude of bulk velocity fluctuations is about the Alfvén velocity since $\delta B \sim B$ in the shock precursor. The Doppler parameter b derived from high resolution UV spectra of the WHIM (see e.g. Lehner et al. 2007; Richter et al. 2008 - Chapter 3, this volume):

$$b^2 = \frac{2T}{m_a} + b_{\text{nt}}^2$$

would have in the micro-turbulent limit a non-thermal contribution

$$b_{\text{nt}}^2 = \frac{2v_{\text{turb}}^2}{3} = \frac{C_\nu B^2}{6\pi \langle \rho \rangle \delta}.$$

The factor C_ν here accounts for the amplitude and spectral shape of the turbulence. For a strong MHD-turbulence that was found in the recent models of strong collisionless shocks with efficient particle acceleration (e.g. Vladimirov et al. 2006) one can get $C_\nu \sim 1$ in the WHIM, and then

$$b_{\text{nt}} \approx 4B_{-9}(\Omega_b h^2 / 0.02)^{-1/2} (1+z)^{-3/2} \delta^{-1/2} \text{ km s}^{-1}.$$

The estimation of b_{nt} given above for a strong Alfvén turbulence may be regarded as an upper limit for a system with a modest MHD turbulence. The non-thermal Doppler parameter does not depend on the ion mass, but $b_{\text{nt}} \propto \delta^{-1/2} B(z)$. Thus the account of b_{nt} could be important for high resolution spectroscopy of metal lines, especially if the strong shocks can indeed highly amplify local magnetic fields. That is still to be confirmed, but a recent high resolution observation of a strong Balmer-dominated shock on the eastern side of Tycho’s supernova remnant with the *Subaru Telescope* supports the existence of a cosmic ray shock precursor where gas is heated and accelerated ahead of the shock (Lee et al. 2007). High resolution UV spectroscopy of the WHIM could allow to constrain the intergalactic magnetic field. Internal shocks in hot X-ray clusters of galaxies have modest Mach numbers and the effect of the Alfvén turbulence is likely less prominent than that in the strong accretion shocks in clusters and in the cosmic web filaments. X-ray line broadening by large scale bulk motions in the hot intracluster medium was discussed in detail by Fox & Loeb (1997) and Inogamov & Sunyaev (2003).

4 Ionisation state of the WHIM

To simulate absorption spectra of bright quasars in the intervening WHIM filaments (e.g. Kawahara et al. (2006) as an example of such a modelling) one should solve the ionisation balance equations for the charge states of metal ions with account taken of all the LTE processes and also the nonthermal particle contribution (see Porquet et al. (2001) for a discussion of a role of non-relativistic super-thermal distributions). The ionisation balance equation can be written as

$$\begin{aligned} \dot{n}_q = & n_e [n_{q-1}C_{q-1} - n_q C_q - n_q \alpha_q + n_{q+1} \alpha_{q+1}] + \\ & + \sum_{j=\text{H, He, He}^+} n_j [n_{q-1} V_{j,q-1}^{\text{ion}} - n_q (V_{j,q}^{\text{rec}} + V_{j,q}^{\text{ion}}) + n_{q+1} V_{j,q+1}^{\text{rec}}] + \\ & + n_{q-1} R_{q-1} - n_q R_q. \end{aligned}$$

Here q is the charge state of an element, C_q is the collisional (and autoionisation) rate $q \rightarrow q+1$, α_q are the radiative and the dielectronic ionisation rates $q \rightarrow q-1$ (in $\text{cm}^3 \text{s}^{-1}$), $V_{j,q}^{\text{rec}}$, $V_{j,q}^{\text{ion}}$ are the charge exchange rates with the ion j (in $\text{cm}^3 \text{s}^{-1}$) and R_q is the photoionisation rate of an ion (in s^{-1}). The rates of different processes can be calculated for different temperature regimes (see Kaastra et al. 2008 - Chapter 9, this volume). We just limit our discussion here to one example of such a simulation.

In Fig. 4 we illustrate *collisional ionisation equilibrium* curves of oxygen ions in the present epoch (at $z = 0$) as a function of WHIM density δ . The various boundaries

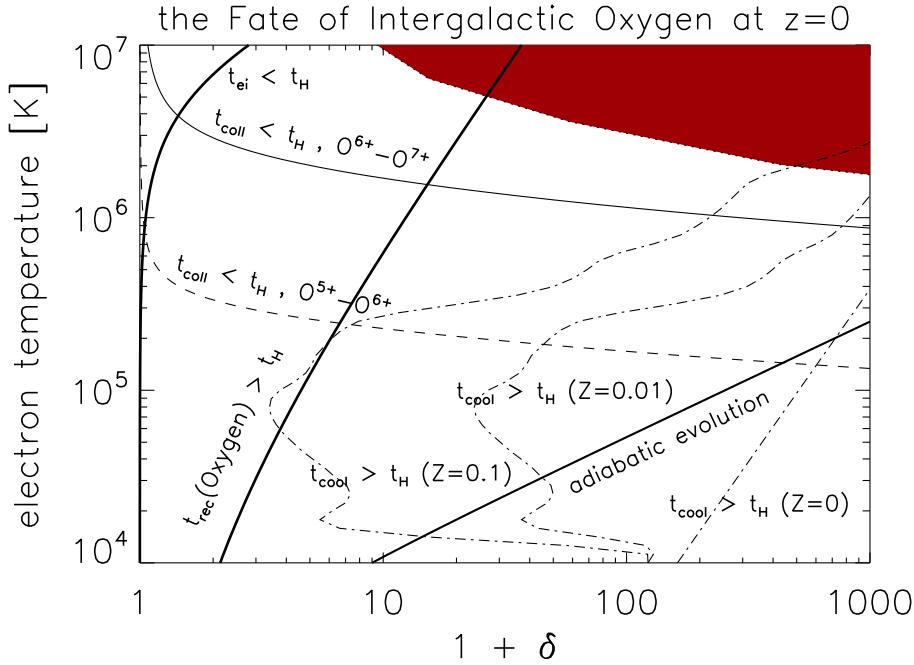


Fig. 4 Phase diagram for oxygen in the IGM at redshift $z = 0$. Density is parameterised by the δ value as was defined above. The solid line in the upper left hand corner labelled ' $t_{ei} < t_H$ ' indicates where electron and proton fluids reach equilibrium in a Hubble time (t_H). Low density gas will not radiatively cool over a Hubble time to the left of the boundaries marked ' $t_{cool} > t_H$ '. The three curves are labelled with the metallicity, Z , expressed as a fraction of Solar metallicity. The solid curve labelled '*adiabatic evolution*' indicates the locus of gas that has only undergone adiabatic compression or expansion since high redshift (initial condition $T_e \sim 10^4$ K). Critical boundaries for the ionisation equilibrium of oxygen are: the shaded area in the upper right hand corner indicates the regime where the collisional ionisation timescale is shorter than the photoionisation timescale, for ionisation $O_{VIII} \rightarrow O_{IX}$. The two boundaries labelled ' $t_{coll} < t_H$ ' indicate where the collisional ionisation timescale becomes shorter than the Hubble time. At lower temperature, the ionisation balance cannot be in (collisional) equilibrium. Upper (solid) curve is for ionisation $O_{VII} (O^{+6}) \rightarrow O_{VIII} (O^{+7})$, lower (dashed) curve for $O_{VI} (O^{+5}) \rightarrow O_{VII} (O^{+6})$. The steep solid curve labelled ' $t_{rec}(\text{Oxygen}) > t_H$ ' indicates where the radiative recombination timescale ($O_{IX} \rightarrow O_{VIII}$) exceeds the Hubble time (no recombination at low densities).

separate regimes under which a certain process does, or does not attain equilibrium over a Hubble time. We show in Fig. 4 some critical boundaries for kinetic and thermal equilibrium. The solid line in the upper left hand corner labelled ' $t_{ei} < t_H$ ' indicates where electron and proton fluids reach kinetic equilibrium (proton temperature equal to electron temperature) in a Hubble time (t_H): at low density and high temperature, such equilibrium does not attain. Low density gas will not radiatively cool over a Hubble time to the left of the boundaries marked ' $t_{cool} > t_H$ '. The cooling time was calculated for collisionally ionised gas. The solid curve labelled '*adiabatic evolution*' indicates the locus of gas that has only undergone adiabatic compression or expansion since high redshift (initial condition $T_e \sim 10^4$ K); all shock-heated gas will be above

this line right after passing through a shock. The shaded area in the upper right hand corner indicates the regime where the collisional ionisation timescale is shorter than the photoionisation timescale, for ionisation O VIII \rightarrow O IX. The two boundaries labelled ' $t_{\text{coll}} < t_{\text{H}}$ ' indicate where the collisional ionisation timescale becomes shorter than the Hubble time. At lower temperature, the ionisation balance cannot be in (collisional) equilibrium. The steep solid curve labelled ' $t_{\text{rec}}(\text{Oxygen}) > t_{\text{H}}$ ' indicates where the radiative recombination timescale (O IX \rightarrow O VIII) exceeds the Hubble time since there is no recombination at low densities.

Note that we illustrate here only the collisional equilibrium case. For the more appropriate case of radiative cooling in photoionisation equilibrium, the cooling times will be even longer, due to the fact that a photoionised plasma is highly overionised compared to the characteristic ionisation- and excitation potentials, which suppresses the (very effective) collisional cooling contribution. In our figure, the lines $t_{\text{cool}} = t_{\text{H}}$ will shift to the right if we calculate with the probably more realistic case of photoionisation equilibrium. However, as we argued above the collisional equilibrium is also of interest, since it represents a conservative case. The range of ionisation states of oxygen in the WHIM filaments can be observed in the absorption spectra of bright quasars.

5 Conclusions

We discussed some specific features of the WHIM heating processes by collisionless plasma shocks driven by gravitationally accelerated flows in the LSS structure formation scenario.

- Collisionless shock heating of ions in the WHIM results in a highly non-equilibrium initial state with a strongly anisotropic quasi-Maxwellian ion distribution just behind a very thin magnetic ramp region. The ion temperatures just behind the shock depend on the ion atomic weight, the charge state and the shock magnetic field inclination. The ion temperatures could decline from a simple linear scaling with the ion mass providing an excessive heating of heavy ions.

- The ion and electron temperatures relax to the equilibrium state through Coulomb collisions in a layer of the depth $N_{\text{eq}} \sim 10^{16} v_7^4 \text{ cm}^{-2}$ behind a shock of velocity v_7 .

- Strong collisionless plasma shocks with an efficient Fermi acceleration of energetic particles can generate strong MHD waves in the downstream region that will result in a non-thermal broadening of the emission/absorption lines in the observed WHIM spectra.

Acknowledgements The authors thank ISSI (Bern) for support of the team “Non-virialized X-ray components in clusters of galaxies”. A.M.B. thanks M. Yu. Gustov for his help with hybrid shock simulations, he acknowledges the RBRF grant 06-02-16844 and a support from RAS Presidium Programs. A support from NASA ATP (NNX07AG79G) is acknowledged.

References

- Bell, A. R. 2004, MNRAS, 353, 550
 Blandford, R. & Eichler, D. 1987, Phys. Rep., 154, 1
 Burgess, D., Lucek, E. A., Scholer, M., et al. 2005, SSR, 118, 205
 Bykov, A., Dolag, K., & Durret, F. 2008, SSR, in press

-
- Bykov, A. M. 2005, *Advances in Space Research*, 36, 738
- Bykov, A. M. & Uvarov, Y. A. 1999, *JETP*, 88, 465
- Cen, R. & Ostriker, J. P. 1999, *ApJ*, 514, 1
- Cen, R., Tripp, T. M., Ostriker, J. P., & Jenkins, E. B. 2001, *ApJ*, 559, L5
- Davé, R., Cen, R., Ostriker, J. P., et al. 2001, *ApJ*, 552, 473
- Durret, F., Kaastra, J. S., Nevalainen, J., Ohashi, T., & Werner, N. 2008, *SSR*, in press
- Fang, T., Bryan, G. L., & Canizares, C. R. 2002, *ApJ*, 564, 604
- Farris, M. H., Russell, C. T., Thomsen, M. F., & Gosling, J. T. 1992, *J. Geophys. Res.*, 97, 19121
- Fox, D. C. & Loeb, A. 1997, *ApJ*, 491, 459
- Furlanetto, S. R., Schaye, J., Springel, V., & Hernquist, L. 2004, *ApJ*, 606, 221
- Ghavamian, P., Laming, J. M., & Rakowski, C. E. 2007, *ApJ*, 654, L69
- Hellsten, U., Gnedin, N. Y., & Miralda-Escudé, J. 1998, *ApJ*, 509, 56
- Ichimaru, S. & Rosenbluth, M. N. 1970, *Phys. Fluids*, 13, 2778
- Inogamov, N. A. & Sunyaev, R. A. 2003, *Astronomy Letters*, 29, 791
- Kaastra, J. S., Paerels, F. B. S., Durret, F., Schindler, S., & Richter, P. 2008, *SSR*, in press
- Kaastra, J. S., Werner, N., den Herder, J. W. A., et al. 2006, *ApJ*, 652, 189
- Kaiser, T. B. 1979, *Phys. Fluids*, 22, 593
- Kang, H., Ryu, D., Cen, R., & Ostriker, J. P. 2007, *ApJ*, 669, 729
- Kawahara, H., Yoshikawa, K., Sasaki, S., et al. 2006, *PASJ*, 58, 657
- Kennel, C. F., Edmiston, J. P., & Hada, T. 1985, *Geophys. Monograph Ser.*, 34, 1
- Korreck, K. E., Zurbuchen, T. H., Lepri, S. T., & Raines, J. M. 2007, *ApJ*, 659, 773
- Lee, J.-J., Koo, B.-C., Raymond, J., et al. 2007, *ApJ*, 659, L133
- Lee, L. C. & Wu, B. H. 2000, *ApJ*, 535, 1014
- Lehner, N., Savage, B. D., Richter, P., et al. 2007, *ApJ*, 658, 680
- Lembege, B., Giacalone, J., Scholer, M., et al. 2004, *SSR*, 110, 161
- Levinson, A. 1996, *MNRAS*, 278, 1018
- Markevitch, M. & Vikhlinin, A. 2007, *Phys. Rep.*, 443, 1
- Mewe, R. 1990, in *Physical Processes in Hot Cosmic Plasmas*, ed. W. Brinkmann, A. C. Fabian, & F. Giovannelli (Kluwer), 39
- Nicastro, F., Mathur, S., Elvis, M., et al. 2005, *Nature*, 433, 495
- Paerels, F. B. S. & Kahn, S. M. 2003, *ARAA*, 41, 291
- Porquet, D., Arnaud, M., & Decourchelle, A. 2001, *A&A*, 373, 1110
- Raymond, J. C. 2001, *SSR*, 99, 209
- Richter, P., Paerels, F. B. S., & Kaastra, J. S. 2008, *SSR*, in press
- Schwartz, S. J., Thomsen, M. F., Bame, S. J., & Stansberry, J. 1988, *J. Geophys. Res.*, 93, 12923
- Sivukhin, D. V. 1966, in *Reviews of Plasma Physics*, Vol. 4, 93
- Spitzer, L. 1962, *Physics of Fully Ionized Gases* (Interscience, New York (2nd ed.))
- Takei, Y., Henry, J. P., Finoguenov, A., et al. 2007, *ApJ*, 655, 831
- Tripp, T. M., Savage, B. D., & Jenkins, E. B. 2000, *ApJ*, 534, L1
- Vainshtein, S. I., Bykov, A. M., & Toptygin, I. 1993, *Turbulence, current sheets, and shocks in cosmic plasma* (Gordon & Breach)
- Vladimirov, A., Ellison, D. C., & Bykov, A. 2006, *ApJ*, 652, 1246